Dipolar mixtures in checkerboard optical bilayers

Rukmani Bai [1,2,*] and Luis Santos [1,†]

[1]*Institut für Theoretische Physik, Leibniz Universität Hannover, Appelstrasse 2, D-30167 Hannover, Germany*

[2]*Centre for Quantum Science and Technology (CQST), International Institute of Information Technology Hyderabad, Gachibowli, Hyderabad, Telangana 500032, India*

(Received 28 July 2026; accepted 9 October 2026; published 29 October 2026)

Ultracold dipolar mixtures in component-dependent optical potentials constitute an interesting platform for the study of the interplay between intra- and intercomponent anisotropic long-range interactions. We study the particular case of binary dipolar mixtures placed in separated bilayers which are displaced in an antimagic wavelength configuration. Using a combination of second-order perturbation theory and cluster-Gutzwiller calculations, we unveil a rich landscape of possible crystalline phases for the two components, showing that, interestingly, intersite hopping may result, via superexchange, in solid-into-solid transitions between different crystalline phases. These crystalline phases and the corresponding transitions can be experimentally realized using, e.g., lanthanide mixtures in optical lattices.

DOI: 10.1103/35j8-4tr1

I. INTRODUCTION

Recent years have shown a surge in the interest on dipolar quantum gases, formed by particles with large magnetic or electric dipole moments. Due to the anisotropic long-range character of the dipole-dipole interaction, these gases present a qualitatively new physics compared to the nondipolar counterparts [1–3]. Milestone experiments on dipolar Bose-Einstein condensates have revealed a very rich physics, including rotonlike excitations [4], dipolar droplets [5,6], and dipolar supersolidity [7–9].

Dipolar gases in optical lattices provide an excellent platform for the study of the interplay of short- and long-range interactions in many-body lattice models. In particular, itinerant dipoles in optical lattices or tweezer arrays allow for the quantum simulation of extended Hubbard models [1,2,10], characterized by strong intersite interactions which may extend well beyond nearest-neighboring sites. These interactions are expected to result in a rich ground-state physics and nonequilibrium dynamics. Recent experiments using highly magnetic erbium atoms have recently observed for the first time the formation of density waves with checkerboard or stripe configurations [11], which stem directly from the anisotropic intersite dipole-dipole interaction.

Recent experiments on dipolar mixtures open intriguing possibilities for the study of the competition between intra- and intercomponent dipolar interactions [12–21]. Interestingly, experiments on lanthanides allow for component-selective optical addressing [17], allowing for the study of scenarios in which the two components experience a different optical lattice. Particularly interesting is the case of binary mixtures in a one-dimensional antimagic wavelength configuration, in which one component experiences a one-dimensional lattice displaced by half a unit cell compared to the other component, which may be employed, e.g., for the realization of frustrated lattice models [22].

In this paper, we consider the particular case of a 2D antimagic wavelength (checkerboard) configuration, in which each component is placed in a square lattice, but one lattice is displaced half a unit cell in each direction on the lattice plane. Moreover, the two lattices have a vertical displacement, forming a bilayer system; see Fig. 1(a). By a combination of second-order perturbation theory and cluster Gutzwiller ansatz calculations, we show that this particularly simple arrangement reveals for hard-core dipolar bosons a rich ground-state landscape characterized by different crystalline geometries that depend on the dipole orientation and the interlayer separation. Interestingly, the tunneling itself may induce a solid-into-solid transition between two different crystalline phases, as a result of superexchange processes.

The paper is organized as follows. In Sec. II, we introduce the model and the cluster Gutzwiller method. Section III discusses the phase diagram when the dipoles are oriented perpendicular to the layer planes. In Sec. IV we discuss the case in which the dipoles have a component on the layer planes. Finally, in Sec. V, we summarize our conclusions.

II. MODEL AND METHOD

We consider a binary mixture of hard-core dipolar bosons in a component-dependent checkerboardlike bilayer setup as that of Fig. 1(a). Component $\kappa = 1, 2$ remains confined in layer κ. The layers are separated by a distance h along the z axis. Both components experience a square optical lattice (we consider the lattice constant as the length unit), but they are in antimagic wavelength configuration such that the lattice of

*Contact author: rukmani.bai@itp.uni-hannover.de

†Contact author: santos@itp.uni-hannover.de

Published by the American Physical Society under the terms of the Creative Commons Attribution 4.0 International license. Further distribution of this work must maintain attribution to the author(s) and the published article's title, journal citation, and DOI.

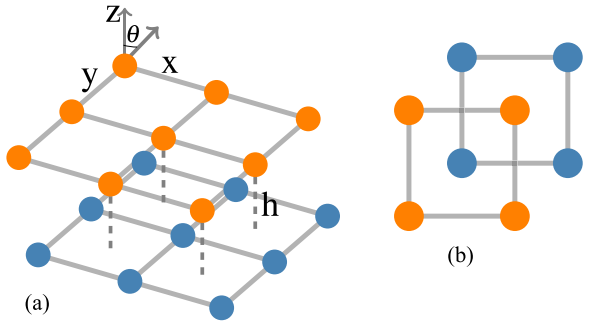


FIG. 1. (a) Scheme of the considered bilayer square-lattice setup. The layers are separated by a vertical distance h. Each layer is occupied by only one of the components. (b) Scheme of the considered 2×2 cluster, with four sites in each layer, employed in our CGW calculations.

layer 2 is shifted by half a lattice constant in each direction compared to that of layer 1; see Fig. 1(a). The system is described by the extended Bose-Hubbard Hamiltonian:

$$\hat{H} = -J \sum_{\langle i,j\rangle,\kappa} \hat{b}^{\dagger}_{i,\kappa}\hat{b}_{j,\kappa} - \sum_{i,\kappa} \mu_{\kappa}\hat{n}_{i,\kappa} + \frac{1}{2}\sum_{i\neq j,\kappa} V^{i,j}_{\kappa,\kappa}\hat{n}_{i,\kappa}\hat{n}_{j,\kappa} + \sum_{i,j} V^{i,j}_{1,2}\hat{n}_{i,1}\hat{n}_{j,2}, \quad (1)$$

where $\kappa = \{1, 2\}$, $\hat{b}^{\dagger}_{j,\kappa}$ ($\hat{b}_{j,\kappa}$) is the creation (annihilation) of a boson at site j of layer κ, $\hat{n}_{j,\kappa} = \hat{b}^{\dagger}_{j,\kappa}\hat{b}_{j,\kappa}$, $(\hat{b}^{\dagger}_{j,\kappa})^2 = 0$, J is the nearest-neighbor intralayer hopping rate, which we assume for simplicity to be the same for both components, and μ_{κ} is the chemical potential for component κ. Assuming that an external field orients the dipoles on the xz plane along the direction $\mathbf{e}_d = (\sin\theta, 0, \cos\theta)$, the dipole-dipole interaction between site i at layer κ and site j at layer κ' is given by

$$V^{i,j}_{\kappa,\kappa'} = \frac{V_{\kappa,\kappa'}}{|\mathbf{r}_{i,\kappa} - \mathbf{r}_{j,\kappa'}|^3}\left(1 - 3\frac{(\mathbf{e}_d \cdot (\mathbf{r}_{i,\kappa} - \mathbf{r}_{j,\kappa'}))^2}{|\mathbf{r}_{i,\kappa} - \mathbf{r}_{j,\kappa'}|^2}\right). \quad (2)$$

We assume for simplicity $V_{1,1} = V_{2,2} = V_{1,2} = V$, which we consider our energy scale, and assume $\mu_1 = \mu_2 = \mu$ such that both components have equal population. Here $\mathbf{r}_{j,1} = (j_x, j_y, 0)$ and $\mathbf{r}_{j,2} = (j_x + 1/2, j_y + 1/2, h)$.

We are interested in the ground-state properties of the two-component bilayer system. The transition between superfluid and insulating phases may be well studied by means of cluster Gutzwiller (CGW) ansatz calculations [23–25] (tunneling-induced solid-into-solid transitions are in contrast not well resolved using CGW, as discussed below). In CGW, the square lattice is split in each layer into clusters of $M \times N$ sites (along x and y, respectively). The ground state is written as a product state of clusters: $|\Psi_{\mathrm{CGW}}\rangle = \bigotimes_c |\psi\rangle_c$, where the cluster state is expressed as a linear combination of Fock states: $|\psi\rangle_c = \sum_{\mathbf{n},\mathbf{m}} f^c_{\mathbf{n},\mathbf{m}}|\mathbf{n}, \mathbf{m}\rangle_c$, where $\mathbf{n} = \{n_1, n_2, \ldots, n_{M\times N}\}$ for the first species and $\mathbf{m} = \{m_1, m_2, \ldots, m_{M\times N}\}$ for the second one. We then approximate: $\hat{H} \simeq \sum_c (\hat{H}_c + \hat{H}^{\mathrm{MF}}_c)$, such that

$$\hat{H}_c = -J \sum_{\langle i,j\rangle\in c,\,\kappa} \hat{b}^{\dagger}_{i,\kappa}\hat{b}_{j,\kappa} - \sum_{i\in c,\kappa} \mu_{\kappa}\hat{n}_{i,\kappa} + \frac{1}{2}\sum_{(i\neq j)\in c,\,\kappa} V^{i,j}_{\kappa,\kappa}\hat{n}_{i,\kappa}\hat{n}_{j,\kappa} + \sum_{(i,j)\in c} V^{i,j}_{12}\hat{n}_{i,1}\hat{n}_{j,2} \quad (3)$$

is the exact Hamiltonian within the cluster c [26], whereas the hopping and interactions with neighboring clusters are considered in mean field:

$$\hat{H}^{\mathrm{MF}}_c = \sum_{i\in c,\,\kappa} [-J\eta_{i,\kappa}(\hat{b}^{\dagger}_{i,\kappa} + \hat{b}_{i,\kappa}) + \beta_{i,\kappa}\hat{n}_{i,\kappa}], \quad (4)$$

where $\eta_{i,\kappa} \equiv \sum_{\langle j\in c'\neq c\rangle_i} \phi_{j,\kappa}$ (with $\langle j \in c' \neq c\rangle_i$ denoting the neighboring sites to site i which do not belong to cluster c), $\beta_{i,\kappa} \equiv \sum_{j\in c'\neq c}(V^{i,j}_{\kappa,\kappa}\rho_{j,\kappa} + V^{i,j}_{1,2}\rho_{j,\kappa'\neq\kappa})$, and we have introduced the superfluid order parameter $\phi_{j,1} = \langle\Psi_{\mathrm{CGW}}|\hat{b}_{j,1}|\Psi_{\mathrm{CGW}}\rangle = \sum_{\mathbf{n},\mathbf{m}} \sqrt{n_j} f^{c\,*}_{\mathbf{n}-\mathbf{e}_j,\mathbf{m}} f^c_{\mathbf{n},\mathbf{m}}$, and the average occupancy $\rho_{j,1} = \langle\Psi_{\mathrm{CGW}}|\hat{n}_{j,1}|\Psi_{\mathrm{CGW}}\rangle = \sum_{\mathbf{n},\mathbf{m}} n_j |f^c_{\mathbf{n},\mathbf{m}}|^2$, and similarly for the component 2. We perform our CGW calculations on a bilayer system with 8×8 lattice sites per layer, which we split into 2×2 clusters, i.e., each cluster has eight sites, with four in each layer; see Fig. 1(b). We consider periodic boundary conditions along both x and y.

III. DIPOLES PERPENDICULAR TO THE LAYERS

We start our analysis with the case in which the dipoles are aligned along the z direction. We focus first on the atomic limit, $J = 0$, and incorporate below the nontrivial effect of hopping. Figure 2(a) depicts the lattice filling on each layer ($\rho_{1,2} = \rho$) as a function of the chemical potential μ and the interlayer separation h. Increasing μ/V leads to an h-dependent sequence of different lattice fillings. In this paper, we focus on half filling, $\rho = 1/2$, and hence for each value of h we consider a chemical potential along the solid line in Fig. 2(a).

In the atomic limit, the ground state is a Fock state with given occupations $n_{i,\kappa}$, which minimize the interaction energy:

$$E = \frac{1}{2}\sum_{i\neq j,\kappa} V^{i,j}_{\kappa,\kappa} n_{i,\kappa} n_{j,\kappa} + \sum_{i,j} V^{i,j}_{1,2} n_{i,1} n_{j,2}. \quad (5)$$

The competition between intra- and interspecies interactions leads to the emergence of various crystalline phases, with characteristic occupation patterns and vanishing superfluid order parameter. For sufficiently weak interspecies interaction, i.e., sufficiently large separation h, the ground state is characterized by a checkerboardlike filling of each layer. In this checkerboard (CB) phase, the population of both components align, forming a characteristic filamentlike pattern; see Fig. 2(b). As h decreases the interspecies interaction strength increases and the ground state of the binary mixture undergoes a transition to a crystalline phase characterized by alternated two-rows-wide stripes of each component. This two-row stripe (2ST) phase is sketched in Fig. 2(d). Interestingly, as shown in Fig. 2(c), at the transition, the CB and 2ST phases are quasidegenerate (the energy difference is $\Delta E \simeq 0.004V$), with yet a third crystalline arrangement, which we denote as the intermediate crystalline (CRS) phase. This crystal presents the intricate geometry depicted in Fig. 2(c). Finally, for sufficiently small separation h, the repulsive interspecies interaction becomes significantly stronger than the intraspecies interaction and the system transitions into a phase-separated (PS) state; see Fig. 2(e). We should point out that the results were evaluated for a relatively small 8×8 lattice. For large system sizes, the 2ST-PS transition shifts and occurs via other

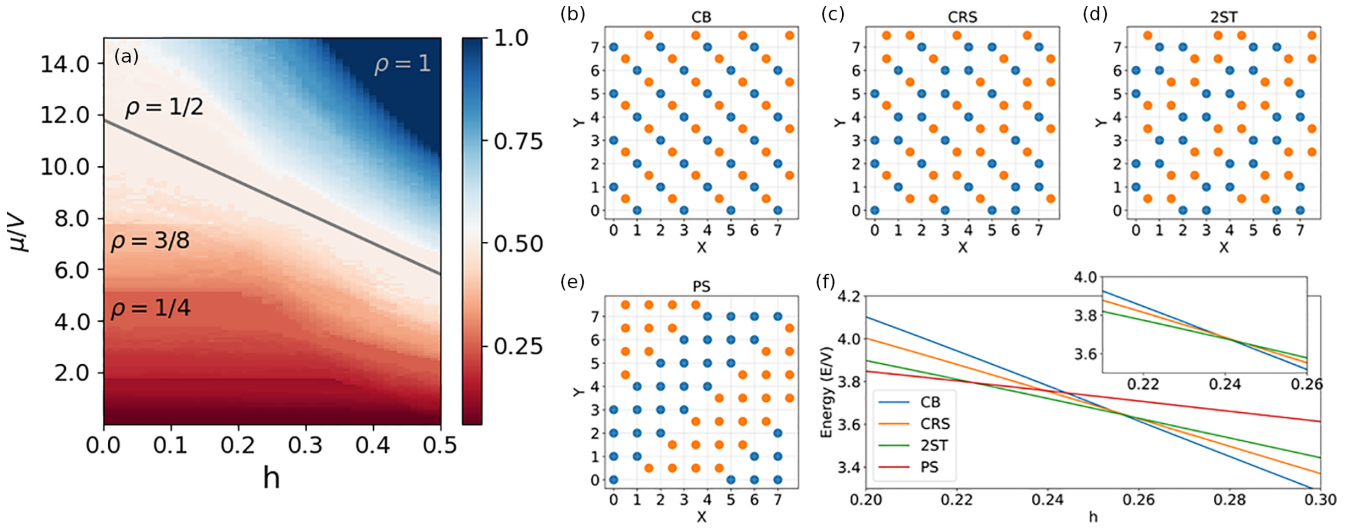


FIG. 2. (a) Density $\rho_{1,2} = \rho$ as a function of the interlayer spacing h and the chemical potential μ. We focus on $\rho = 1/2$, considering chemical potentials along the solid line. (b) Checkerboard (CB) crystal. (c) Intermediate crystalline (CRS) phase. (d) Two-row stripe (2ST) phase; (e) phase separated (PS) phase: here it is limited due to the 8×8 lattice with periodic boundary conditions; larger lattices show the formation of broader domains. (f) Energy of the different crystalline phases in the atomic limit ($J = 0$) as a function of h. In the inset, we show the energy of the CB, CRS, and 2ST phases as a function of h for $J/V = 0.2$, showing that, also at finite hopping, the three phases remain approximately degenerate at the CB-2ST transition.

intermediate stripe phases [e.g., for a 16×16 lattice, we observe a very narrow intermediate region (in between 2ST and PS) with a stripe phase formed by alternated four-row stripes of each component].

A finite particle hopping eventually results not only in crystal melting into a superfluid phase, but also in solid-into-solid transitions (i.e., transitions between different crystal geometries), induced by superexchange processes [27,28]. The latter result from virtual hops, which affect in a different way the various crystal geometries. For each one of the phases depicted in Figs. 2(b)–2(e), we evaluate the energy shift ΔE associated with the hopping of a single particle into an empty neighboring site. This virtual hopping process results in a second-order energy shift $-J^2/\Delta E$. Adding up the contribution of all particles, we evaluate the overall change in the energy per particle for the phase $\alpha =$ CB, ST, CRS, and PS, from its atomic limit value $E_{\alpha;0}(h, V)$ to $E_\alpha(h, V, J) = E_{\alpha,0}(h, V) - \gamma_\alpha(h, V)J^2/V$; for details see Appendix A. Superexchange induces the shift of the phases, resulting in tunneling-induced CB-2ST and PS-2ST transitions, as depicted in Fig. 3.

Solid-into-solid transitions are not well reproduced by CGW methods. This is because hops between different clusters are evaluated in mean field and are hence canceled in crystalline phases [$\eta_{i,\kappa} = 0$ in Eq. (4)]. As a result, calculations with 2×2 (4×2) clusters are characterized by an effective coordination number $z_{\text{eff}} = 2$ (2.5) and not of $z = 4$. This point is illustrated in Fig. 3(a), where we show that the evaluated 2ST-CB boundary for 2×2 (4×2) clusters coincides with the correct results evaluated in second-order perturbation, when employing $J_{\text{eff}} = 2(1.6)J$; see Appendix B.

Very large clusters would be necessary to reproduce the actual solid-to-solid transition, rendering the CGW treatment of the tunneling-induced solid-into-solid transitions numerically unfeasible. We hence evaluate those transitions using the superexchange calculation. In contrast this problem does not affect significantly the crystal-to-superfluid transitions and hence we use CGW to determine the melting transitions into a superfluid phase, characterized by homogeneous density and finite superfluid order parameter. Using this combination of methods we obtain the phase diagram depicted in Fig. 3(b). We employ this procedure in all other results discussed below.

Interestingly, although the intermediate CRS phase is strictly speaking never the ground state, its energy remains at finite hopping quasidegenerate with that of the CB and 2ST crystals in the vicinity of the CB-2ST transition [see inset of Fig. 2(f)]. Indeed, we observe this phase in our CGW calculation and we expect that it would appear as well as the metastable solution in experiments.

The hopping-induced solid-to-solid transition results in a distortion of the insulator $\rho = 1/2$ lobe in the (J, μ) phase diagram, as depicted in Fig. 3(c). Upon leaving the $\rho = 1/2$ lobe, the 2ST phase transitions into a regime of metastable (MS) states, characterized by no superfluid parameter or density order and by a fluctuating density pattern from run to run (we perform simulations with up to 10 different random initial conditions). The CB phase transitions into a SF or a checkerboard supersolid (SS) phase. The latter phase is characterized by a modulated density and finite superfluid order parameter.

IV. ANISOTROPIC DIPOLAR INTERACTION WITH POLARIZATION ANGLE

Up to this point we have only considered dipoles along z ($\theta = 0$). For $\theta \neq 0$, the dipoles have a projection along x, hence breaking the isotropy of the xy plane. Figure 4(a) shows the phase diagram as a function of the separation h and the orientation angle θ in the atomic limit, $J/V \to 0$. When θ grows the intracomponent interaction along x becomes eventually

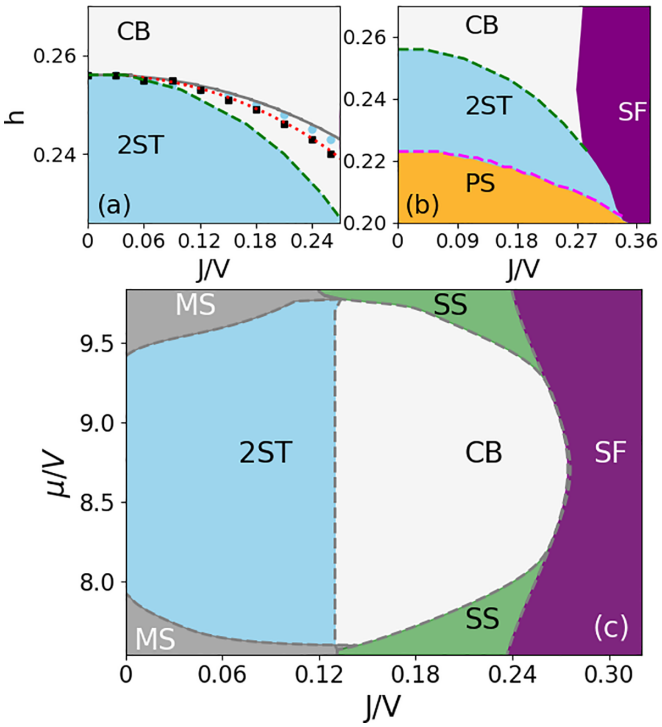


FIG. 3. (a) CB-2ST transition. The dashed line indicates the CB-2ST transition as obtained from the second-order perturbation theory calculation. As expected, see text, the second-order results with $J_{\text{eff}} = 2J$ (solid curve) match with the CGW calculation for a 2×2 lattice (filled circles), whereas the CGW results for a 4×2 lattice (filled squares) match with the second-order results using $J_{\text{eff}} = 1.6J$ (dotted curve). This result shows both that the second-order perturbation theory is valid at the J values considered and that CGW cannot be employed to determine the solid-into-solid transitions. (b) Phase diagram as a function of the hopping J and the interlayer separation h, assuming the dipoles oriented perpendicularly to the layer ($\theta = 0$). (c) Phase diagram for $h = 0.25$ as a function of J and the chemical potential μ; we depict the lobe of $\rho = 1/2$ and its vicinity. The lobe presents a super-exchange-induced solid-into-solid 2ST-CB transition. Associated to this transition there is a change in the nature of the phases outside the lobe, which include a supersolid (SS) checkerboard phase.

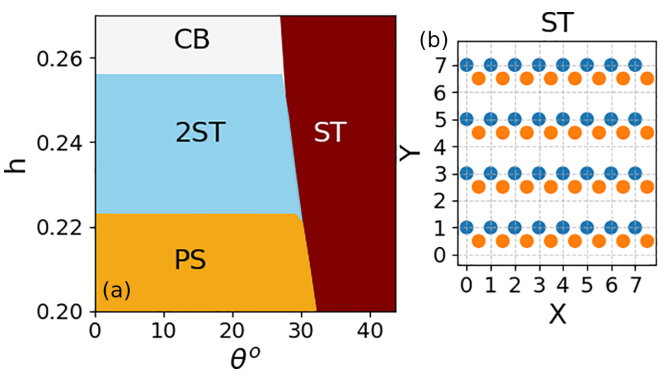


FIG. 4. (a) Phase diagram in the atomic limit ($J = 0$) as a function of the dipole orientation θ and the interlayer spacing h. (b) Stripe (ST) phase characteristic of large-enough angles θ.

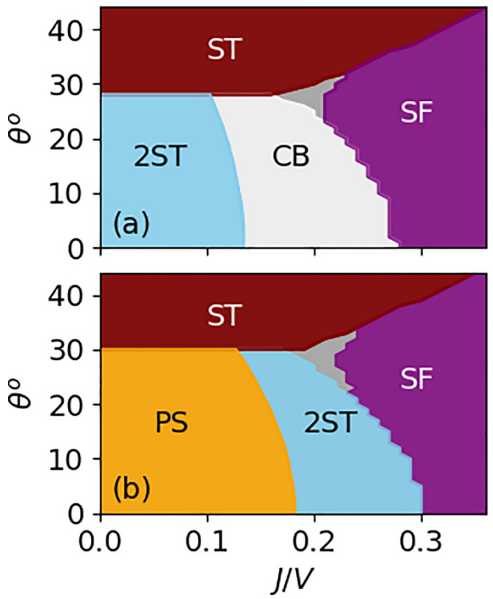


FIG. 5. Phase diagram as a function of the hopping J and the orientation angle θ for $h = 0.25$ (a) and $h = 0.217$ (b). Note the solid-into-solid transitions, as well as the significant dependence of the crystal-to-superfluid transition depending on the orientation angle. The gray zone indicates amorphous metastable solutions in our CGW calculations.

attractive for $\theta > \arcsin(1/\sqrt{3})$, while remaining repulsive along y. As a result, the ground-state undergoes a phase transition at a critical $\theta_c(h)$ from the isotropic ground-state crystals discussed in the previous section (PS, 2ST, CB) into the stripe (ST) phase, where particles align in stripes along x, formed by two rows, one of each component; see Fig. 4(b).

Hopping results, also for $\theta \neq 0$, in solid-into-solid 2ST-CB and PS-2ST transitions for $\theta < \theta_c(h)$, see Figs. 5, which we obtain again employing second-order perturbation theory. Due to the hopping induced transition, at θ_c the system presents a triple point ST-2ST-CB (ST-PS-2ST) point. Increasing J/V eventually drives a θ-dependent crystal melting into a superfluid. The crystal-to-superfluid transition presents a marked θ dependence. At the critical $\theta_c(h)$ the SF penetrates down to small J/V values. In the triple point region CB-ST-SF (2ST-ST-SF) our CGW results show the appearance of metastable states, with random density distribution and finite superfluid order parameter (gray areas in the figures).

V. CONCLUSION

Ultracold dipolar mixtures in component-dependent optical potentials open interesting perspectives for the study of the rich physics that results from the interplay between intra- and intercomponent interactions. Using a combination of second-order perturbation theory and cluster-Gutzwiller calculations, we have analyzed the case of binary mixtures in a bilayer setup with optical lattices in antimagic wavelength (checkerboard) configuration. Whereas, as recently observed experimentally [11], single-component dipoles in square lattices present a transition from checkerboard to stripe phases as a function of the dipole orientation, the ground states of the

considered bilayer geometry depend both on the dipole orientation and on the separation between the layers. This results in a richer landscape of possible crystalline phases for the two components; see Figs. 2(b)–2(e) and 4(b). Interestingly, the hopping itself may result, via superexchange, in solid-into-solid transitions between different crystalline phases. These crystalline phases and the corresponding transitions can be experimentally realized using ultracold lanthanides in optical lattices [10,11]. Lanthanide mixtures are not only dipolar, but also allow for the creation of component-selective optical potentials, due to their available narrow optical transitions [17]. A Dy/Dy mixture, employed in very recent experiments [21,29], would allow for $V_{11} = V_{22} = V_{12}$, although in our work we have chosen this for simplicity.

Finally, we point out that the antimagic-wavelength (checkerboard) bilayer potentials discussed in this paper only illustrate partially the possibilities of a dipolar bilayer setup. Particularly interesting would be to extend ideas recently developed concerning the generation of twisted-bilayer geometries [30,31] to the dipolar case, which may permit the study of the interplay between twisting and dipolar interactions.

ACKNOWLEDGMENTS

We acknowledge the support of the Deutsche Forschungsgemeinschaft (DFG, German Research Foundation), Project-ID No. 274200144, SFB 1227 DQ-mat within the project A04, and under Germany's Excellence Strategy, EXC-2123 Quantum-Frontiers, Grant No. 390837967. R.B. acknowledges the support from Ramanujan Fellowship (File No. RJF/2026/000084) from the Anusandhan National Research Foundation (ANRF), India.

DATA AVAILABILITY

There are no publicly available research data or software supporting this manuscript. Requests for further information or data should be sent to the authors.

APPENDIX A: SECOND-ORDER ENERGY CORRECTION

In this Appendix, we describe the details of the second-order perturbation theory used in the paper.

In the atomic limit $J = 0$, the ground state is a Fock state $|\Psi\rangle = |\{n_{i,\kappa}\}\rangle$, which corresponds to one of the crystalline phases discussed in the text, with an interaction energy

$$E_0(\{n_{i,\kappa}\}) = \frac{1}{2}\sum_{\kappa=1,2}\sum_{i,j\neq i} V^{i,j}_{\kappa,\kappa} n_{i,\kappa} n_{j,\kappa} + \sum_{i,j} V^{i,j}_{1,2} n_{i,1} n_{j,2}. \tag{A1}$$

In order to evaluate the second-order energy correction we first operate with the hopping Hamiltonian on the crystalline state:

$$\hat{H}_T|\Psi\rangle = -J\sum_{\kappa}\sum_{i,\delta}|\Psi_{\kappa,i,\delta}\rangle, \tag{A2}$$

where $|\Psi_{\kappa,i,\delta}\rangle$ is the state in which a single particle in layer κ has hopped from site i to site $i+\delta$. The sum goes over all sites which are occupied in the ground state.

In order to evaluate the energy difference associated with a single hop, we first evaluate for the original crystalline structure the interaction energy of the particle at site i in layer κ with all other particles,

$$E'_{i,\kappa} = \sum_{j\neq i} V(\mathbf{r}_{j,\kappa} - \mathbf{r}_{i,\kappa}) + \sum_{j} V(\mathbf{r}_{j,\kappa'\neq\kappa} - \mathbf{r}_{i,\kappa}), \tag{A3}$$

and then calculate the interaction energy of the particle when it has hopped into a neighboring empty place $\mathbf{r}_{i+\delta,\kappa}$,

$$E''_{i+\delta,\kappa} = \sum_{j} V(\mathbf{r}_{j,\kappa} - \mathbf{r}_{i+\delta,\kappa}) + \sum_{j} V(\mathbf{r}_{j,\kappa'\neq\kappa} - \mathbf{r}_{i+\delta,\kappa}) - V(\mathbf{r}_{i+\delta,\kappa} - \mathbf{r}_{i,\kappa}), \tag{A4}$$

where again the sums go over the sites occupied in the original crystalline state. The second-order energy contribution of that hop is then $\Delta E_{i,\delta,\kappa} = -J^2/dE_{i,\delta,\kappa}$, with $dE_{i,\delta,\kappa} = E''_{i+\delta,\kappa} - E'_{i,\kappa}$. The total energy correction of the crystalline state is hence given by adding the contribution of all possible hops:

$$\Delta E = \sum_{\kappa}\sum_{i,\delta}\Delta E_{i,\delta,\kappa}. \tag{A5}$$

Hence the energy of the crystalline state in the presence of weak hopping may be approximated as $E = E_0 + \Delta E$. We consider that the crystalline structure is such that $E'_{i,\kappa} = E'$ is the same for all sites (this is so for CB, 2ST, and PS phases). We can then write

$$E_0 = \frac{1}{2}\sum_{\kappa}\sum_{i} E'_{i,\kappa} = NE', \tag{A6}$$

with N the number of particles in one layer, which we consider to be the same in both layers. Further, the energy change due to any hop is for CB, 2ST, and PS and also the same $dE_{i,\delta,\kappa} = dE$. Then the energy correction due to all hops is

$$\Delta E = -2NZ\frac{J^2}{dE}, \tag{A7}$$

with Z the number of empty neighboring sites in the same layer in the original crystalline state. We may now evaluate the total energy per particle of the crystalline phase:

$$\epsilon = \frac{E}{2N} = \frac{E'}{2} - Z\frac{J^2}{dE}. \tag{A8}$$

Different crystalline phases present different E', dE, and Z. In our calculation we calculate E' and dE numerically for a fixed interlayer separation h. For example, for $h = 0.25$,

$$\epsilon_{\mathrm{CB}} \simeq 3.70 - 1.22\frac{J^2}{V}, \tag{A9}$$

$$\epsilon_{\mathrm{2ST}} \simeq 3.67 - 0.58\frac{J^2}{V}. \tag{A10}$$

The CB-2ST transition is given by $\epsilon_{\mathrm{CB}} = \epsilon_{\mathrm{2ST}}$, which leads, when evaluated for different h values, to the figure depicted in Fig. 3. The transition between 2ST and PS phases can be evaluated in the same way. A similar procedure can be applied to the CRS phase as well, although in that case the procedure is more involved, since each particle and particle hop must be considered separately, since not all of them are characterized by the same energy.

APPENDIX B: EFFECTIVE COORDINATION NUMBER

The reasoning behind the effective coordination number introduced in Sec. III may be well understood for the CB case from Fig. 6. In Fig. 6(a) we depict the case of a 2×2 cluster. Note that the particles may hop to the four neighbors ($z = 4$). However, in the cluster Gutzwiller approach, hops out of the cluster (dashed lines) are accounted for in mean-field theory. For crystalline phases, the corresponding mean-field contribution vanishes. As a result, the hops along the dashed lines vanish in this formalism. The effective coordination number is hence reduced to $z_{\text{eff}} = 2$. A similar reasoning may be applied to Fig. 6(b), where we consider the case of a 4×2 cluster. Removing the hops along the dashed lines results in an average effective coordination number $z_{\text{eff}} = 2.5$. Applying the same reasoning to the 2ST crystal results in the same effective coordination numbers.

Due to this effective coordination number, if we want to retrieve the same hopping per particle, the hopping must be changed into J_{eff}, such that $z_{\text{eff}} J_{\text{eff}} = zJ$, with $z = 4$. Thus, for the 2×2 (4×2) clusters, we obtain $J_{\text{eff}} = 2(1.6)J$, as discussed in Sec. III.

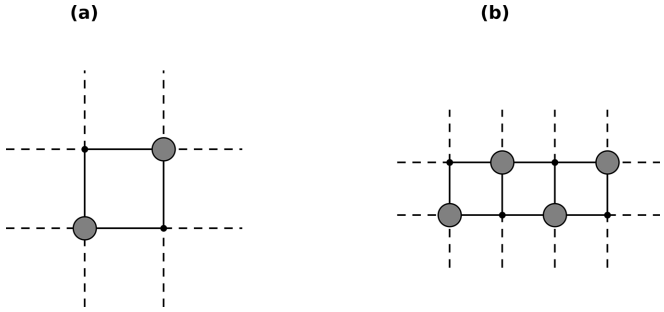


FIG. 6. Suppression of hopping for CB phase for (a) 2×2 cluster and (b) 4×2 cluster.

[1] T. Lahaye, C. Menotti, L. Santos, M. Lewenstein, and T. Pfau, The physics of dipolar bosonic quantum gases, Rep. Prog. Phys. **72**, 126401 (2009).

[2] M. A. Baranov, M. Dalmonte, G. Pupillo, and P. Zoller, Condensed matter theory of dipolar quantum gases, Chem. Rev. **112**, 5012 (2012).

[3] L. Chomaz, I. Ferrier-Barbut, F. Ferlaino, B. Laburthe-Tolra, B. L. Lev, and T. Pfau, Dipolar physics: A review of experiments with magnetic quantum gases, Rep. Prog. Phys. **86**, 026401 (2023).

[4] L. Chomaz, R. M. W. van Bijnen, D. Petter, G. Faraoni, S. Baier, J. H. Becher, M. J. Mark, F. Wächtler, L. Santos, and F. Ferlaino, Observation of roton mode population in a dipolar quantum gas, Nat. Phys. **14**, 442 (2018).

[5] H. Kadau, M. Schmitt, M. Wenzel, C. Wink, T. Maier, I. Ferrier-Barbut, and T. Pfau, Observing the Rosensweig instability of a quantum ferrofluid, Nature (London) **530**, 194 (2016).

[6] S. Zhang, W. Yuan, N. Bigagli, H. Kwak, T. Karman, I. Stevenson, and S. Will, Observation of self-bound droplets of ultracold dipolar molecules, Nature (London) **651**, 601 (2026).

[7] L. Tanzi, E. Lucioni, F. Famà, J. Catani, A. Fioretti, C. Gabbanini, R. N. Bisset, L. Santos, and G. Modugno, Observation of a dipolar quantum gas with metastable supersolid properties, Phys. Rev. Lett. **122**, 130405 (2019).

[8] F. Böttcher, J.-N. Schmidt, M. Wenzel, J. Hertkorn, M. Guo, T. Langen, and T. Pfau, Transient supersolid properties in an array of dipolar quantum droplets, Phys. Rev. X **9**, 011051 (2019).

[9] L. Chomaz, D. Petter, P. Ilzhöfer, G. Natale, A. Trautmann, C. Politi, G. Durastante, R. M. W. van Bijnen, A. Patscheider, M. Sohmen, M. J. Mark, and F. Ferlaino, Long-lived and transient supersolid behaviors in dipolar quantum gases, Phys. Rev. X **9**, 021012 (2019).

[10] S. Baier, M. J. Mark, D. Petter, K. Aikawa, L. Chomaz, Z. Cai, M. Baranov, P. Zoller, and F. Ferlaino, Extended Bose-Hubbard models with ultracold magnetic atoms, Science **352**, 201 (2016).

[11] L. Su, A. Douglas, M. Szurek, R. Groth, S. F. Ozturk, A. Krahn, A. H. Hébert, G. A. Phelps, S. Ebadi, S. Dickerson, F. Ferlaino, O. Marković, and M. Greiner, Dipolar quantum solids emerging in a Hubbard quantum simulator, Nature (London) **622**, 724 (2023).

[12] A. de Paz, A. Sharma, A. Chotia, E. Maréchal, J. H. Huckans, P. Pedri, L. Santos, O. Gorceix, L. Vernac, and B. Laburthe-Tolra, Nonequilibrium quantum magnetism in a dipolar lattice gas, Phys. Rev. Lett. **111**, 185305 (2013).

[13] A. Trautmann, P. Ilzhöfer, G. Durastante, C. Politi, M. Sohmen, M. J. Mark, and F. Ferlaino, Dipolar quantum mixtures of erbium and dysprosium atoms, Phys. Rev. Lett. **121**, 213601 (2018).

[14] G. Durastante, C. Politi, M. Sohmen, P. Ilzhöfer, M. J. Mark, M. A. Norcia, and F. Ferlaino, Feshbach resonances in an erbium-dysprosium dipolar mixture, Phys. Rev. A **102**, 033330 (2020).

[15] Y. A. Alaoui, B. Zhu, S. R. Muleady, W. Dubosclard, T. Roscilde, A. M. Rey, B. Laburthe-Tolra, and L. Vernac, Measuring correlations from the collective spin fluctuations of a large ensemble of lattice-trapped dipolar spin-3 atoms, Phys. Rev. Lett. **129**, 023401 (2022).

[16] C. Politi, A. Trautmann, P. Ilzhöfer, G. Durastante, M. J. Mark, M. Modugno, and F. Ferlaino, Interspecies interactions in an ultracold dipolar mixture, Phys. Rev. A **105**, 023304 (2022).

[17] F. Claude, L. Lafforgue, J. J. A. Houwman, M. J. Mark, and F. Ferlaino, Optical manipulation of spin states in ultracold magnetic atoms via an inner-shell hz transition, Phys. Rev. Res. **6**, L042016 (2024).

[18] P. Barral, M. Cantara, L. Du, W. Lunden, J. de Hond, A. O. Jamison, and W. Ketterle, Suppressing dipolar relaxation in thin layers of dysprosium atoms, Nat. Commun. **15**, 3566 (2024).

[19] M. Lecomte, A. Journeaux, J. Veschambre, J. Dalibard, and R. Lopes, Production and stabilization of a spin mixture of ultracold dipolar Bose gases, Phys. Rev. Lett. **134**, 013402 (2025).

[20] T. Lauprêtre, J. D. Bernal, Y. Baamara, A. M. Rey, L. Vernac, and B. Laburthe-Tolra, Probing coherences and itinerant magnetism in a dipolar lattice gas, Phys. Rev. Lett. **136**, 103401 (2026).

[21] S. Nie, Z. Jiang, J. Huang, X. Luo, F. Qin, K. Wang, and M. Guo, Binary dipolar condensates of dysprosium isotopes with tunable spatial order, arXiv:2606.26606.

[22] M. Miotto, P. Lombardi, G. Ferioli, J. Fraxanet, M. Lewenstein, L. Tanzi, and L. Barbiero, Flux magnetism in a strongly interacting dipolar lattice supersolid under tunable gauge fields, Phys. Rev. Lett. **137**, 043401 (2026).

[23] R. Bai, S. Bandyopadhyay, S. Pal, K. Suthar, and D. Angom, Bosonic quantum Hall states in single-layer two-dimensional optical lattices, Phys. Rev. A **98**, 023606 (2018).

[24] S. Bandyopadhyay, H. Sable, D. Gaur, R. Bai, S. Mukerjee, and D. Angom, Quantum phases of dipolar bosons in a multilayer optical lattice, Phys. Rev. A **106**, 043301 (2022).

[25] D.-S. Lühmann, Cluster Gutzwiller method for bosonic lattice systems, Phys. Rev. A **87**, 043619 (2013).

[26] In our CGW calculations, we determine the dipole-dipole interaction between two sites as given by the shortest distance, taking into account periodic boundary conditions.

[27] P. W. Anderson, Antiferromagnetism. Theory of superexchange interaction, Phys. Rev. **79**, 350 (1950).

[28] T. Mendes-Santos, R. Mondaini, T. Paiva, and R. R. dos Santos, Kaleidoscope of phases tuned by global dipole orientations in the Hubbard model, Phys. Rev. B **108**, 205128 (2023).

[29] M. Dürbeck, L. Reihs, J. P. Marulanda-Serna, B. Choudhari, J. Seifert, N. Werum, G. Meijer, and G. Valtolina, Dipolar Bose-Bose mixture of dysprosium isotopes with controllable interspecies interactions, Phys. Rev. A **114**, L031301 (2026).

[30] A. González-Tudela and J. I. Cirac, Cold atoms in twisted-bilayer optical potentials, Phys. Rev. A **100**, 053604 (2019).

[31] Z. Meng, L. Wang, W. Han, F. Liu, K. Wen, C. Gao, P. Wang, C. Chin, and J. Zhang, Atomic Bose–Einstein condensate in twisted-bilayer optical lattices, Nature (London) **615**, 231 (2023).